

GT2011-4) , ,

A NUMERICAL INVESTIGATION OF MOMENT COEFFICIENT AND FLOW STRUCTURE IN A ROTOR-STATOR CAVITY WITH ROTOR MOUNTED BOLTS

Elham Roshani Moghaddam, Daniel Coren, Christopher Long and Abdulnaser Sayma

Thermo-Fluid Mechanics Research Centre
 University of Sussex, Brighton, BN1 9QT, U.K.

ABSTRACT

This paper presents a numerical study of the effect of rotor mounted bolts on the moment coefficient and flow structure within a rotor-stator cavity representative of modern gas turbine engine design. The CFD computations are performed using the commercial code FLUENT. The simulation methodology is first validated using experimental data from plain co-rotating disc and rotor-stator cavities from the open literature. Comparisons are then made with experimental data obtained from a test rig at the Thermo Fluid Mechanics Research Centre (TFMRC), University of Sussex. Computations were performed at $Re_\phi = 6.8 \times 10^6$, $C_w = 5929$ ($\lambda_T = 0.35$) with different numbers of bolts ($0 < N < 60$), and also a continuous ring, at $r/b = 0.9$.

The study has improved the current understanding of the effect on moment coefficient and flow structure that rotor mounted protrusions have in rotor-stator systems. It is seen that the contribution of skin friction to the moment coefficient reduces as the number of bolts is increased. The size and shape of the wake created by a rotating bolt also means that the pressure loss per bolt reduces with N but the overall effect is to increase the moment coefficient because there are more bolts.

NOMENCLATURE

a, b Inner and outer radius of the disc, respectively
 D Bolt diameter (measured across-flats)
 $G = s/b$ Gap ratio

M Moment
 \dot{m} Mass flow rate
 N Number of bolts
 p Pressure
 r_s Radius of the shaft
 r, z Radial and axial coordinates
 r_p Radius of the protrusions
 s Axial gap between discs
 s_c Seal clearance
 U Mean radial velocity
 V_r, V_ϕ Radial and tangential velocities in a stationary coordinate system.
 $\beta = V_\phi/\omega r$ Core rotation factor
 β^* Value of β when $C_w = 0$
 μ Dynamic viscosity
 ρ Density
 ω Angular velocity

Fluid Dimensionless Groups

$C_m = \frac{M}{1/2 \rho \omega^2 b^5}$ Moment coefficient
 $C_w = \frac{\dot{m}}{\mu b}$ Flow Reynolds number
 $Re_\phi = \frac{\rho \omega b^2}{\mu}$ Rotational Reynolds number

$$\lambda_T = \frac{C_w}{\text{Re}_\phi^{0.8}} \quad \text{Turbulent flow parameter}$$

1 INTRODUCTION AND REVIEW OF PREVIOUS WORK

Increasing the specific power output of a gas turbine engine, and consequently reducing the size of the power plant for a given power rating, requires a higher turbine entry temperature of the main gas flow. Turbine entry temperatures in modern civil engines are currently above 1600°C, and components in contact with such high temperatures quickly exceed their creep and fatigue limits. It is only possible to operate at these elevated temperatures because of internal air systems which use some of the compressor air to cool the turbine discs, blades and nozzle guide vanes. However, air used for cooling will experience forms of viscous dissipation as it flows over both rotating and stationary surfaces. This parasitic phenomenon is referred to as *windage* which consists of contributions from both form drag and skin friction. A torque needs to be provided to overcome the irreversible windage losses. However, there will also be a torque associated with the so-called pumping losses which occur as a result of the work done by a protrusion changing the angular momentum of the fluid. It is important to make this distinction, because the pumping loss term is isentropic. The sum of the irreversible torque (due to windage) and the reversible torque (due to work) is embodied in the moment coefficient which is defined in Equation (3) below. More accurate predictions of windage offer potential for improved design of the internal air system, with associated increases in thrust and efficiency.

Early investigations of frictional losses due to rotating discs were carried out by Daily and Nece (1960) and Bayley and Owen (1969). These identified a number of relevant dimensionless parameters. For a disc of outer radius, b , rotating at an angular velocity ω , in a fluid of density ρ , and dynamic viscosity μ , supplied with a superimposed mass flow rate \dot{m} , the torque is M . The dimensionless flow rate, C_w , rotational Reynolds number, Re_ϕ and moment coefficient, C_m are defined as.

$$\text{Re}_\phi = \frac{\rho \omega b^2}{\mu} \quad (1)$$

$$C_w = \frac{\dot{m}}{\mu b} \quad (2)$$

$$C_m = \frac{M}{1/2 \rho \omega^2 b^5} \quad (3)$$

For no superimposed flow, $C_w = 0$, the flow structure comprises separate boundary layers on the rotor and stator and a central core region where there is only tangential motion with about 40% of disc speed. Flow is pumped up the rotor and

moves radially inward down the stator. For $C_w > 0$, increasing the superimposed flow reduces the tangential velocity of the core. For small amounts of superimposed flow, the flow structure in the cavity is dominated by rotation; conversely for large amounts, the flow structure is dominated by the superimposed flow. Owen and Rogers (1989) developed a useful parameter to delineate these two regimes. This is the turbulent flow parameter λ_T which takes its definition from Von Kármán's (1921) solution (using a one-seventh power law for the velocity profile) for the flow entrained by a free disc.

$$C_{w,\text{ent}} = 0.219 \text{Re}_\phi^{0.8} \quad (4)$$

and so

$$\lambda_T = \frac{C_w}{\text{Re}_\phi^{0.8}} \quad (5)$$

For $\lambda_T > 0.219$, the flow structure is expected to be dominated by the superimposed flow and for $\lambda_T < 0.219$, rotational effects dominate.

The experiments of Dibelius et al. (1984) used a test rig with a rotor disc in an enclosed housing. For rotor mounted bolts, they noted a significant increase in the moment coefficient above that of a plain disc. This occurred for both zero superimposed flow and large values of superimposed flow. They also noticed that the effect of the protrusions on the flow structure was more pronounced when the flow was dominated by rotational effects.

Zimmerman et al. (1986) measured the effect on shaft torque of various bolt designs. Those considered were: staged (i.e. axially stacked concentric bolts of reducing diameter), cylindrical rotor bolts, partially covered and fully covered (by an annular ring) rotor bolts. It was found that eighteen staged bolts on a disc at a radius ratio, $r_p/b = 0.75$, increased torque by a factor of 2.5, with further increases for cylindrical shaped bolts. Partially covered bolts, gave little benefit in reducing the overall torque compared to the uncovered bolts. However, fully covered bolts, gave a significant reduction in moment coefficient compared with the uncovered bolts and a moment coefficient of approximately 25% above that of a plain disc. The effect of a superimposed flow of $C_w = 2.6 \times 10^4$ was to increase the moment coefficient by 50% for all configurations. The increase in moment coefficient due to protrusions was attributed to the superposition of three elements: form drag, skin friction and pumping losses. They found that for a small number of bolts, form drag dominates the additional moment produced, whereas for a large number of bolts the pumping losses become more important. In addition, they also suggested a theoretical limit where increasing the number of bolts will decrease the moment coefficient.

The experiments of Millward and Robinson (1989) involved measurements of enthalpy rise in supplied flow from varying the number of bolts, their diameter, circumferential pitch, and projected cross sectional area. These bolts were attached to both the rotor, as well as on the stationary casing. They obtained a correlation of their results for protrusions attached to the rotor. They also noted that the effect on enthalpy rise of bolts located towards the outer radius was very significant, whereas those located towards the inner radius had little effect. For protrusions on the stator, there was insufficient data to derive a correlation, but it was noted that the enthalpy rise due to stator bolts was about one-third of the corresponding conditions with rotor bolts. Tests were also carried out with full and partial covering of both stator and rotor bolts. No measurable effect was found by partially covering the rotor bolts but the stator bolts showed a reduction in enthalpy rise at high mass flows. Fully covered bolts, however, gave similar results to a plain disc and in some cases a reduction was actually observed.

Gartner (1997) developed a semi-empirical correlation that gives satisfactory agreement for the moment coefficient from a plain disc over a wide range of dimensionless mass flows. Gartner (1998) used a momentum integral method to predict the frictional torque from a single disc with protrusions. The predictions agree well with available data, providing the spacing between the bolts is not so small that wake effects become significant.

Coren (2007) carried out an experimental study on windage effects in rotor-stator cavities. Tests were carried out with bolts mounted on the rotor or on the stator. He suggested correlations for the moment coefficient as a function of the number, size and location of the bolts. He also used Laser Doppler Anemometry (LDA) to measure the radial and tangential components of velocity.

2 THE BOLT WINDAGE TEST RIG

Figure 1 shows a general assembly of the test rig. This consists of a shaft mounted titanium alloy disc of outer radius $b = 225$ mm enclosed within a sealed steel pressure casing. The maximum clearance between the rotor and casing, $s = 22$ mm. Around the outer rim of the disc is a labyrinth seal and a stator mounted shroud encases the cavities on either side of the disc. The disc is driven by a 50 kW motor through a 5:1 step up gearbox. Mounted between the gearbox and the disc is an in line torque meter. The test side of the disc (labelled 'front cavity' in Figure 1) carries the majority of the instrumentation whereas the balance side (labelled 'rear cavity') has sufficient instrumentation to balance the flow conditions on both sides of the disc. A superimposed flow of air enters the rig centrally on the test side, flows radially outward through the cavity and leaves through the labyrinth seal at the perimeter. An equal amount of air is supplied to the balance side, where the air

enters through four inlet pipes equally spaced around the central shaft. There are four orifice plates positioned upstream and downstream of the test rig on both the test and balance side to measure the mass flow of air through the rig as well as to ensure both sides are balanced. The air is supplied at pressures of up to 7.5 bar (absolute) and mass flows of up to 0.82 kg/s by an Atlas Copco screw type compressor and treated with an Atlas Copco air conditioning unit to provide dry air in the range 15 to 25 °C prior to delivery to the rig.

A shaft mounted Vibrometer TM112 in line torque meter measures torque and rotational speed. The 95% confidence interval in torque measurement is less than ± 1 N m, The uncertainty in speed measurement is less than ± 5 rev / min. The torque due to bearing friction in the test rig depends on rotational speed and was obtained by a previous calibration. This driveline torque was subtracted from all of the measured values of torque to obtain a value of the torque transmitted to the fluid, M . The magnitude of the driveline torque varied from 2% of the total at high rotational speeds to 20% at low values of rotational speed.

It is important to note that the test rig was designed with the intention of making the torque on the test and balance sides equal. The two sides have the same geometrical configuration with bolts located on both sides of the disc at the same radius. Furthermore, the pressure was kept equal on both sides of the cavity to provide the same flow conditions. The cooling flow enters into the balance side at a much higher radius than that on the test side. As a result the flow travels over a smaller section of disc before exiting the system. There are two reasons why this difference in inlet radius is thought to be insignificant. Firstly, the torque on a plain disc is a strong function of radius (von Kármán, $M \propto r^{4.6}$). Consequently, most of the contribution to the torque experienced by the balance side comes from that radially outward of the inlet. Secondly, the tangential velocity of the disc at this higher radius will also be proportionally higher, leading to greater shear between the disc and non rotating fluid near the entry point. This will increase the local moment coefficient in this region which will act to balance the torque experienced on each side of the disc.

Tests were carried out with $N = 3, 9$ and 18 and $D = 16$ mm, hexagonal bolts of height, $H = 11$ mm. These were attached, at a radius of 0.2 m, $r_b/b = 0.889$, to both sides of the disc surface to ensure similar conditions on either side, minimizing axial conduction. The orientation of the bolts relative to the direction of rotation is shown in Figure 2.

3 VALIDATION OF THE COMPUTATIONAL MODEL

Two cases were selected for validation purposes in this study. This choice was based on various considerations, such as

similarity in geometric configuration and flow conditions with the data from the bolt windage test rig as well as the availability of experimental data for the validation cases.

3.1 Validation Case No. 1: Flow in a rotating cylindrical cavity with radial outflow

The experimental data for this validation test case come from Pincombe (1981). Figure 3 shows a schematic diagram of the rotating cylindrical cavity comprising two co-rotating discs of outer radius $b = 443$ mm and separated by an axial distance $s = 59$ mm ($G = s/b = 0.133$). Air at 1 bar and 293 K enters the cavity axially with no swirl through a circular hole of radius $a = 44.3$ mm ($a/b = 0.1$) and leaves the cavity radially through an opening in the shroud. The dimensionless conditions investigated were: $Re_\phi = 10^5$ and $C_w = 1092$. In the experiment, there is peripheral shroud which has 30 holes of 32 mm diameter. For simplicity of modeling, the exit geometry is assumed to be a continuous slot of the same equivalent area as the thirty discrete holes. Figure 4. shows the 3-D configuration of the simulated geometry.

The simulation work for the bolt windage rig is non-axisymmetric. Consequently, all the validation test cases were simulated in 3-D. For the cavity shown here a 10° sector was modeled. As shown in Figure 4, there is an extended geometry after the outlet which is used to avoid reverse flow. This extended geometry provides a uniform flow before the outlet boundary, and prevents it from changing direction and re-entry through the outlet, which could cause numerical problems.

It is common to use an inlet pipe at the entrance of rotating cavities with superimposed flow. The role of this inlet pipe is to provide a fully-developed, low-turbulence velocity profile before entering the cavity. The length of the inlet pipe used here is 1.8 m which provides enough length for forming the fully developed flow ($L/D = 21$).

A grid independence study was carried out in order to make sure that the computational results do not change by producing further refined grids (the finest mesh had 270,000 points)

As shown in Figure 4, unstructured meshes were only used in the plane of the disc surfaces (the $r - \phi$ plane). Meshes were generated for use with enhanced wall treatment in which the first grid near the wall is located in the laminar sub-layer region. The inlet velocity, outlet pressure and rotational speed were calculated from the values of mass flow coefficient and rotational Reynolds number. At the rotational speed of the test rig (7.6 rad/s) the flow can be assumed to be incompressible. Three thousand iterations were required to get a converged solution and a 2nd order discretisation scheme was used for all variables.

As described by Pincombe, for $C_w = 1092$, the flow is expected to be completely turbulent. Therefore the computational results are dependent on the selection of an appropriate turbulence model of the Reynolds Averaged Navier-Stokes equations are used. Accordingly, different turbulence models were examined in order to find the model which can best match the experimental data.

Figure 5 shows the axial variation ($z/s = 0$ corresponds to the surface of the upstream disc) of the radial component of velocity for a number of different turbulence models together with the experimental results of Pincombe. The radial velocity is shown in dimensionless form on the vertical axis as V_r/U where U is a mass-continuity derived radial velocity, defined by:

$$U = \frac{C_w \mu}{2\pi \rho r G} \quad (6)$$

and the horizontal axis is the dimensionless axial coordinate z/s .

As shown in Figure 5, all the turbulence models predict a similar radial velocity distribution across the cavity with differences that are thought to be within the bounds of experimental uncertainty. However, there is a noticeable difference between the predicted and measured values; the experimental results that show a higher maximum radial velocity and a steeper gradient towards the core region. The reason for this is unclear. However the following facts should be noted: the absolute values of this disparity are very small (less than 0.08 m/s); the measurement of this component of velocity is sensitive to small misalignment; the disparity with a $1/7^{\text{th}}$ power law is much greater; and the measurements were made almost thirty years ago with equipment that has been superseded.

Table 2. shows the predicted values of dimensionless tangential velocity $V_\phi/\omega r$ at $z/s = 0.5$ (in the central core) and at $r/b = 0.833$ for different the turbulence models used. As can be seen the predictions of all turbulence models are similar, but the predicted values always exceed that measured experimentally. However, as previously noted the difference in velocity is small (0.17 m/s) in this case and the experimental uncertainties could be relatively significant.

3.2 Validation Test Case No. 2: Flow in a Rotor-Stator Cavity with a Superimposed Radial Outflow

This validation test case examines the flow in a fully shrouded rotor-stator system with a superimposed radial outflow of fluid. Comparison is made with the experimental measurements and computations of Poncet et al. (2005), who used water as the working fluid. The temperature was maintained constant at

23°C, the density and kinematic viscosity of water are taken as 999 kg/m³ and 0.942 10⁻⁶ m²/s respectively. Their measurements were obtained using a two-component Laser Doppler Anemometry system. Measurements were made of the radial and tangential components of velocity for both a superimposed radial inflow and a superimposed radial outflow. However, only the results of the case with radial outflow are used for comparison in this present study. Figure 6 shows a schematic diagram of the cavity where: $s = 9$ mm, $b = 250$ mm ($G = s/b = 0.036$), $a = 54.5$ mm, $r_s = 38$ mm and $s_c = 3$ mm. The comparison here is for $Re_\phi = 1.04 \times 10^6$ and $C_w = 5929$ ($\lambda_T = 0.09$).

In the experiment, water enters axially through the stator and leaves the cavity axially through a radial gap between the rotor and the shroud. The disc adjacent to the inlet (stator) and the shroud are stationary, while the rotor and the shaft are rotating.

In addition to the experimental measurements, Poncet et al. used a numerical method for computing the radial and tangential components of velocity. They used a RSM model which is based on one-point statistical modeling using a low Reynolds number second-order full stress transport closure. Their model is derived from the Launder and Tselepidakis (1994) model and sensitized to rotation effects (Poncet et al., 2005) and is different from the model available in FLUENT used in this study.

Figure 7 shows the 3D geometry of the mesh used to simulate the flow in this rotor stator cavity. As in the previous test case, a 10° sector is simulated. The simulated cavity also has extended geometry at the outlet (for eliminating reverse flow at the exit boundary) and an attached pipe at the inlet (to provide the fully developed flow conditions). The number of points for the grid independent case is 163,000. Meshes were generated to be used with the enhanced wall treatment available in Fluent and 2nd order discretisation was used for all variables.

Figure 8 and 9 compare the current computational results for the axial variation of dimensionless radial and tangential velocities, respectively, at $r/b = 0.56$ with the experimental and numerical results of Poncet et al. The horizontal and vertical axes of Figure 8 are as defined before (z/s and v_r/U , respectively); $z/s = 0$ corresponds to the surface of the stator, and $z/s = 1$ the rotor. For Figure 9, the vertical axis is the nondimensional tangential velocity or swirl ratio, $V_\phi / \omega r$.

The standard K-ε, the realizable K-ε, and the RSM give the closest results to the experimental data. The standard K-ε model was chosen for all further computations due to the lower overhead in processing time. The radial and tangential velocities at two other radial locations of $r/b = 0.44$, and $r/b =$

0.8 are shown in Figure 8 to 13 for the standard K-ε, turbulence model.

The current numerical predictions are in acceptable agreement with both the experimental data on Poncet et al. and also their numerical predictions. Looking at the results shown in Figures 8 to 13 also illustrates some important features of this rotor-stator flow regime. For $r/b = 0.56$ and 0.44 (Figures 9 and 11) there is not a tangential velocity boundary layer on the stator and only on the rotor. The radial velocity at these locations shows evidence of radial outflow only and no recirculation radially inward back down the stator. These features are consistent with what is called a Stewartson Type flow regime. At $r/b = 0.8$ (Figures 12 and 13), this Stewartson Type flow becomes a Batchelor Type flow where there are separate boundary layers on the rotor and stator. Fluid moves radially outward in the rotor boundary layer and radially inward in the stator boundary layer. In Figure 13, there is clear evidence of a core region between the rotor and stator ($0.2 < z/s < 0.8$). The tangential velocity in the core region is usually denoted by the symbol β . For the current numerical predictions at $r/b = 0.8$, $\beta = 0.16$ (the experimental results of Poncet et al. give $\beta = 0.11$ and their numerical predictions give $\beta = 0.2$).

Table 2 compares the simulation results of the rotor moment coefficient for different turbulence models. It can be seen that, except for the RSM, there are no significant differences in the moment coefficient between the different turbulence models. The same result can also be seen in the plot of tangential velocity. This implies that both moment coefficient and tangential velocity are insensitive to the choice of turbulence model used for the simulation. The reason for overestimations of RSM for both the tangential velocity and moment coefficient is because of the constants used for the model in Fluent and the fact that RSM constants needs to be tuned for each special case in the software.

4. THE NUMERICAL MODEL OF THE BOLT WINDAGE RIG

Figure 14 shows part of the 3-D mesh used in the computational model for the bolt windage test rig. The angular extent of the sector simulated depends on the number of bolts. The periodic boundaries of this sector lie mid-way between the bolts, so for 3 bolts a 120° sector is used, for 9 bolts a 40° sector and for 18 bolts a 20° sector. There is an extended geometry at the outlet, and a pipe attached to the inlet. Unstructured grids were used in the r - ϕ plane only. Finer grids are used near the bolt. The distance near the walls were specified so that using the low Reynolds number approach is possible. The number of points in the r - z plane is 180 x 60. The k-epsilon (enhanced wall treatment) model was used for simulations. The pressure and temperature at inlet were set from the experimental data. The outlet pressure was set so that

it produces the amount of fixed mass flow rate. A moving reference frame with an angular velocity of the rotor speed was used. The fluid is taken to be compressible, using the ideal gas for modeling the density, and Sutherland's law (3 coefficient method) for modeling the viscosity. A 2nd order discretisation scheme was used for all variables and a grid independence study was carried out to make sure that the results are not dependent to the mesh quality.

The convergence criteria are as follows:

- 1- Iterations residual for all the variables form a constant horizontal line and are less than 10^{-4} .
- 2- The fluctuations of outlet mass flow rate are less than 0.1% of inlet mass flow rate.
- 3- All monitors are stabilized at least for 1000 iterations (including the moment coefficient and outlet temperature).

The results shown in this paper are for air with a mass flow of 0.415 kg/s, a rotational speed of 409.5 rad/s an inlet pressure of 5 bar and temperature of 296.7 K. The equivalent dimensionless conditions are: $Re_\phi = 6.8 \times 10^6$, $C_w = 10^5$, corresponding to $\lambda_T = 0.35$.

5 ANALYSIS OF RESULTS

Figure 15 shows the variation of moment coefficient (on one side of the disc) with number of bolts N . The experimental results, together with those from the CFD simulations are shown for $N = 3, 9$ and 18 bolts as well as for a plain disc. The plain disc results are indicated by a continuous line for the experimental data and a dashed line for the CFD predictions. Both experimental data and CFD predictions show that, not surprisingly, increasing the number of bolts causes a significant rise in the moment coefficient. As can also be seen from the results shown in Figure 15, there is good overall agreement between the predictions and experimental data and this gives confidence in the numerical model.

Further simulations were carried out for $N = 36, 45, 52$ and 60 (for $N = 60$, the circumferential spacing between one bolt and the next is less than $D/4$) and a continuous ring with 16 mm radial thickness and 11 mm height at $r = 0.2$ m on the rotor. These results are summarised in Figure 16, which again shows the variation of moment coefficient with N .

The CFD results shown in Figure 16 extend the range of those shown in the previous figure and provide a consistent picture of the effect of the number of bolts on the moment coefficient. It is interesting to see from Figure 16 that the moment coefficient of the ring (at $N = 0$) is approximately equal to the moment coefficient of a plane disc. This is in agreement with the investigations of Millward and Robinson (1989).

The effect of the number of bolts on the axial variation of dimensionless tangential velocity is illustrated in Figure 17. The x-axis starts at $z/s = 0.42$ which corresponds to the axial location of the top of the bolt or ring. The tangential velocity varies around the circumference of the bolt radius. The value used in this graph is that obtained at the location of the centreline of the bolt.

It can be seen from Figure 17 that increasing the number of bolts from 9 to 36 causes a significant increase in the tangential velocity. The corresponding change from 36 to 60 bolts is much less and there is very little difference in the tangential velocity when $N \geq 45$. Increasing N is expected to reduce the contribution of skin friction to the total losses since the relative velocity between the fluid and the bolt is reduced (see Fig. 20).

Similar trends occur when the turbulent flow in the wake behind the bolts is examined. This can be seen from Figure 18 which shows contours of Entropy in the region of the bolt radius. It is apparent that the form of the wake changes with the number of bolts fitted to the rotor. Increasing the number of bolts (and decreasing the distance between the two neighbouring bolts) can lead to a situation where the wake of one bolt has not fully collapsed in advance of the following bolt. Although only one condition has been investigated here ($Re_\phi = 6.8 \times 10^6$ and $C_w = 10^5$, $\lambda_T = 0.35$), it is likely that the interference of the wake from one bolt to the next will be dependent on λ_T . This subject will be investigated and reported on in a future publication.

Figure 19 shows contours of relative total pressure in the region of the bolt radius for $N = 9, 18, 45$, and 60 . Increasing the number of bolts, increases the peak total pressure but also decreases the relative total pressure difference across each individual bolt. This leads to a net decrease in the moment due to a single bolt as a consequence of the increased influence of wakes from upstream bolts producing a smaller pressure difference across the bolt. However, since there are more bolts, the contribution of pressure-related moment of all bolts together increases.

Figure 20 shows the contribution of skin friction and pressure-related (form drag and radial pumping) contributions to the overall moment coefficient. It is clear the skin friction contributes less to the overall moment coefficient in comparison with the pressure. As shown in Figure 20, the dominance of the pressure-related moment means that the net effect of increasing the number of bolts is to increase the overall moment coefficient. But for the reasons explained above concerning the structure of the wakes, the rate at which C_m increases with N , decreases as N becomes larger.

It is also worth investigating the influence of bolts on the flow structure in the rotor-stator cavity. Figure 21 shows the velocity streamlines in the r-z plane on the centreline of the bolthead. Two cases are shown: a plain disc and of a cavity with bolt. And it can be seen that the overall flow has a similar structure for both. There is a recirculation of flow near the stator at the inlet, and another near the exit. However, the exit recirculation is larger in the case of the bolt.

CONCLUSIONS

This paper has presented CFD predictions of the flow in a rotor-stator cavity with and without rotor-mounted bolts. Comparison is made with experimental data for $Re_\phi = 6.8 \times 10^6$, $C_w = 10^5$ ($\lambda_T = 0.35$), with $N = 3, 9$ and 18 , 16 mm diameter, 11 mm high hexagonal bolts. The number of bolts in the CFD model has been varied from $0 \leq N \leq 60$ and the contributions of the skin friction and the pressure loss to the overall moment coefficient have been investigated.

The CFD model uses the FLUENT commercial software and a standard K- ϵ turbulence model. The experimental rig comprises a pressurised rotor-stator cavity of the following geometry: $b = 0.225$ m, $s = 0.022$ m, supplied with air.

There is acceptable agreement between the experimental and predicted values of moment coefficient for $N = 3, 9$ and 18 . There is very little difference between the moment coefficient for a continuous ring and that for a plain disc. Increasing the number of bolts brings about an increase in the overall moment coefficient. However, the rate of increase of C_m with N reduces as N gets larger. The tangential velocity between the rotor and stator also increases with N and this causes a reduction in the contribution of skin friction to the overall moment coefficient. The size and shape of the wake formed by a bolts changes with the number of bolts and the wake trailing behind one bolt affects the flow field around a neighbouring bolt. Although the pressure loss per bolt reduces with the number of bolts, the overall effect of increasing N is to increase the overall contribution of pressure loss because there are more bolts.

REFERENCES

- Bayley, F.J., Owen, J.M., 1969, "Flow between a rotating and a stationary disc", *Aeronautical Quarterly*, Vol. 20, pp.333-354.
- B. E. Launder and D. P. Tselepidakis, 1994. "Application of a new second moment closure to turbulent channel flow rotating in orthogonal mode," *Int. J. Heat Fluid Flow* 15, 2.
- Coren, D., 2007. Windage due to Protrusions in Rotor-Stator Systems, D.Phil. thesis, Thermo-Fluid Mechanics Research Centre, University of Sussex, Brighton, UK.
- Daily, J. W. and Nece, R. E. Chamber dimension effects on induced flow and frictional resistance of enclosed rotating discs. *J. Basic Eng.*, 1960, 82, 217–232.
- Dibelius, G., Radtke, F., Ziemann, M., 1984. Experiments on Friction, Velocity and Pressure Distribution of Rotating Discs, Heat and mass transfer in rotating machinery. (A86-24451 09-34), Washington, DC, Hemisphere Publishing Corp., pp. 117-130.
- Gartner, W. 1997 A Prediction Method for the Frictional Torque of a Rotating Disc in a Stationary Housing with a Superimposed Radial Outflow. ASME Gas Turbine and Aeroengine Congress and Exposition, Paper No. 97-GT-204.
- Gartner, W., 1998. A Momentum Integral Method to Predict the Frictional Torque of a Rotating Disc with Protruding Bolts, ASME conference paper, 98-GT-138.
- Millward, J.A., Robinson, P.H., 1989. Experimental Investigation into the Effects of Rotating and Static Bolts on Both Windage Heating and local Heat Transfer Coefficients in a Rotor-Stator Cavity, Gas turbine and aeroengine congress and exposition paper, 89-GT-196.
- Owen, J. M., Rogers, R. H., 1989, "Flow and Heat Transfer in Rotating-Disc Systems." Volume one – Rotor-Stator Systems, Research Studies Press Ltd., ISBN 0 86380 090 4.
- Pincombe, J.R., 1981. Velocity Measurements in the MKII – Rotating Cavity Rig with a Radial Outflow. Report No. 81/TFMRC/21, Thermo-Fluid Mechanics Research Centre, University of Sussex, Brighton, UK.
- Poncet, S., Chauve, M.P., Schiestel, R., 2005. "Batchelor versus Stewartson flow structures in a rotor-stator cavity", *Physics Of Fluids*, 17, 075110,
- von Kármán, T., 1921, "Technical Memorandum on Laminar and Turbulent Friction", National advisory committee for aeronautics, Report No. 1092.
- Zimmerman, H., Firsching, A., Dibelius, G.H., Ziemann, M., 1986. Friction Losses and Flow Distribution for Rotating Discs with Shielded and Protruding Bolts, ASME conference paper, 86-GT-158.

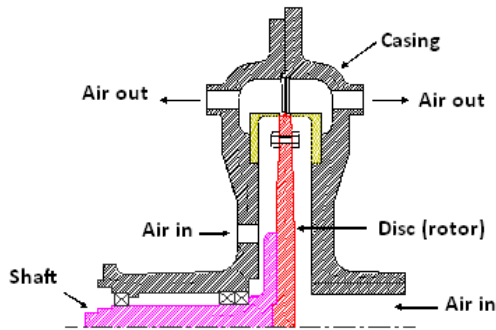
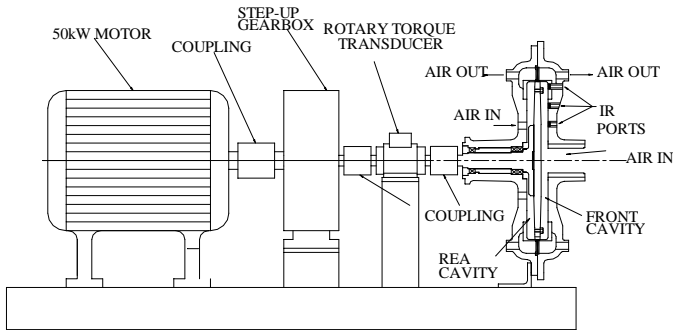


Figure 1. Schematic Diagram of the Bolt Windage Test Rig

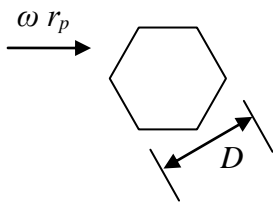


Figure 2 Orientation of Bolts with Respect to Rotation.

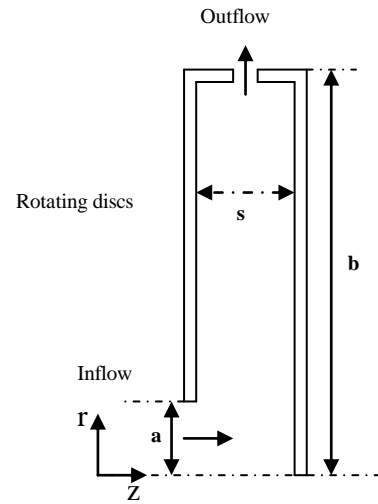


Figure 3 Schematic Diagram of Validation Test Case No. 1: Rotating Cylindrical Cavity with Radial Outflow

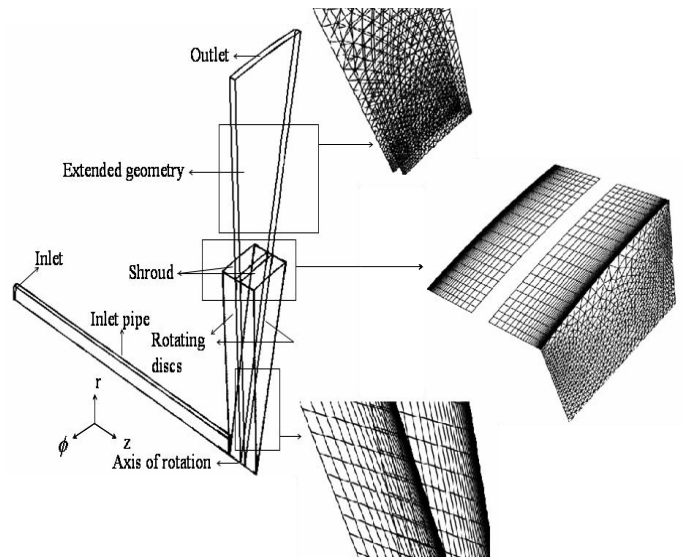
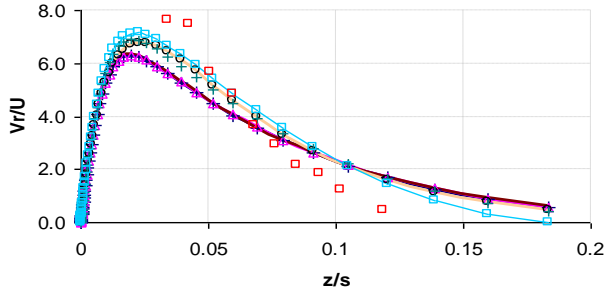


Figure 4. The Numerical Grid for Validation Test Case No. 1



- K-epsilon-Standard
- K-epsilon-RNG
- + K-omega-SST
- Experimental data-Pincombe(1981)
- K-epsilon-Realizable
- RSM
- K-omega-Standard

Figure 5. Validation Test Case No. 1. Axial Variation of radial velocity at $r/b=0.833$ using Different Turbulence Models and Comparison with Experimental Data

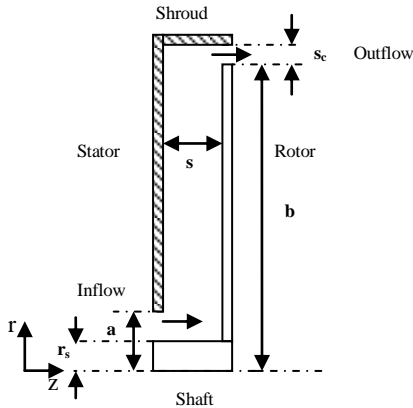


Figure 6. Validation Test Case No. 2, Schematic Configuration of the Cavity with Relevant Notation

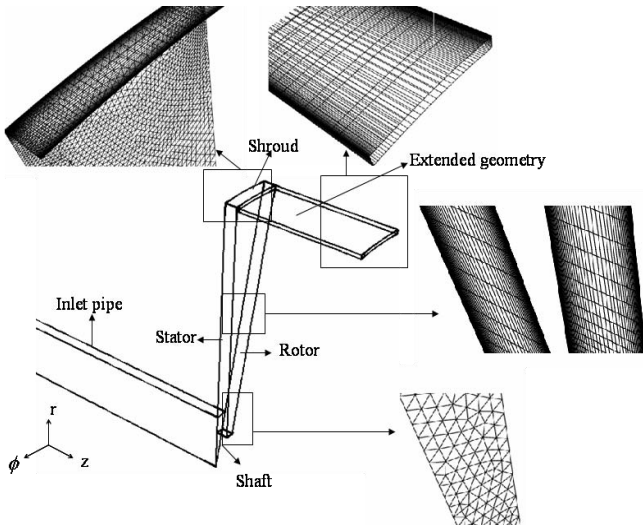
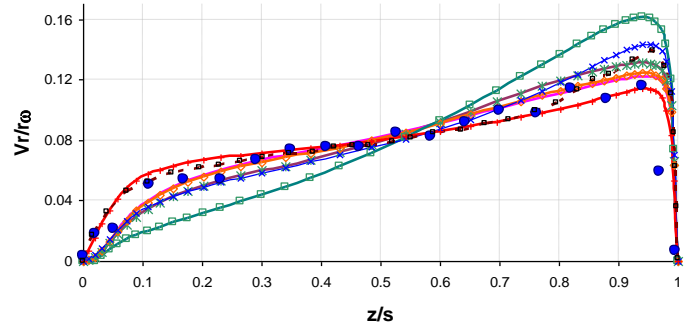
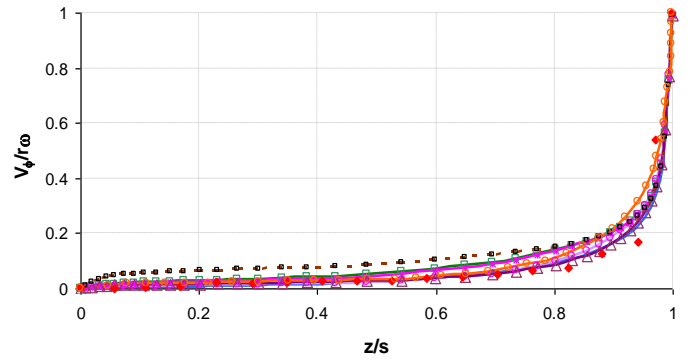


Figure 7. The Numerical Grid for Validation Test Case No. 2



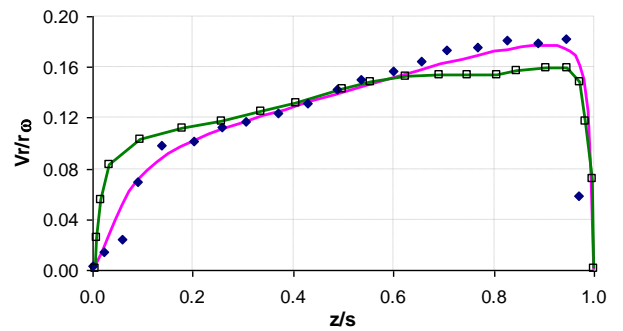
- K-epsilon-RNG
- K-epsilon-Standard
- K-epsilon-Realizable
- K-Omega-SST
- K-Omega-standard
- RSM
- Experimental data-Poncet et al.(2005)
- Numerical-Poncet et al.(2005)

Figure 8. Axial Variation of Radial Velocity at $r/b = 0.56$ Using Different Turbulence Models



- K-epsilon-Standard
- K-epsilon-RNG
- K-epsilon-Realizable
- K-Omega-Standard
- K-Omega-SST
- RSM
- ◆ Experimental data-Poncet et al.(2005)
- Numerical-Poncet et al.(2005)

Figure 9. Axial Variation of Tangential Velocity at $r/b = 0.56$ Using Different Turbulence Models.



- ◆ Experimental data -Poncet et al.(2005)
- Standard K-epsilon
- Numerical-Poncet et al.(2005)

Figure 10. Axial Variation of Radial Velocity at $r/b = 0.44$.

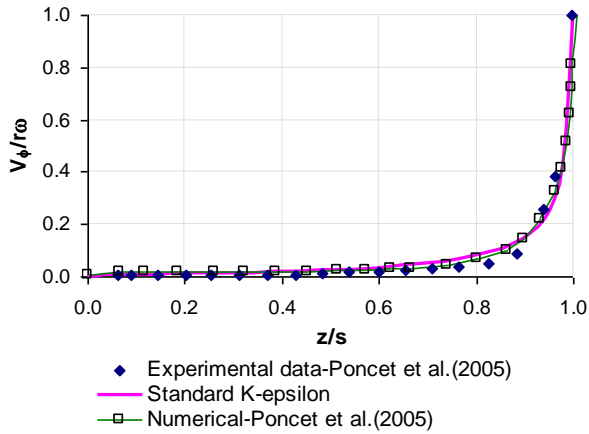


Figure 11. Axial Variation of Tangential Velocity at $r/b = 0.44$

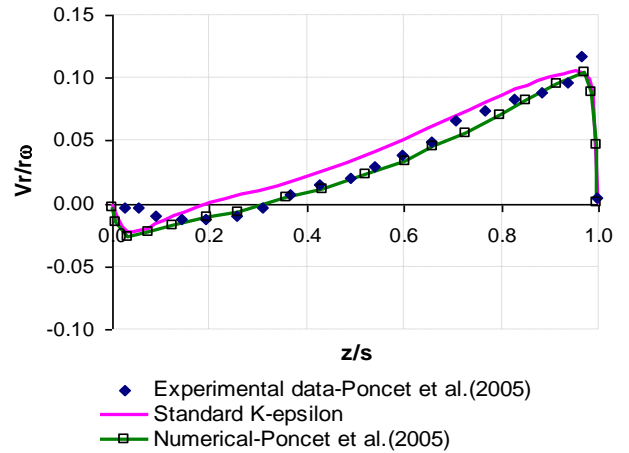


Figure 12. Axial Variation of Radial Velocity at $r/b = 0.8$.

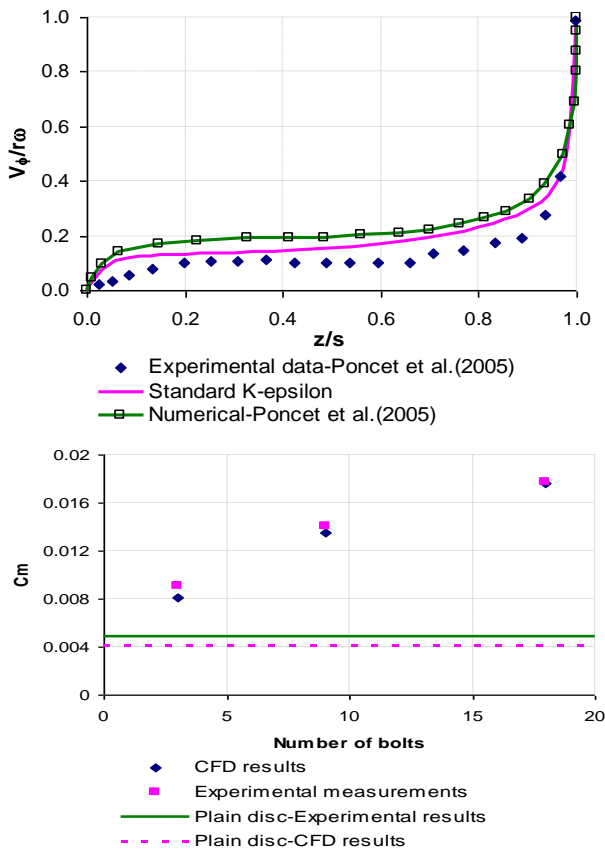


Figure 13. Axial Variation of Tangential Velocity at $r/b = 0.8$.

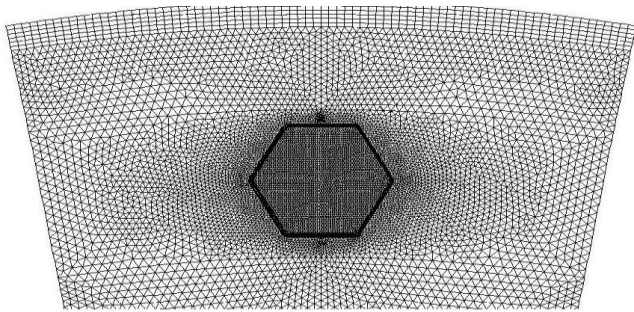
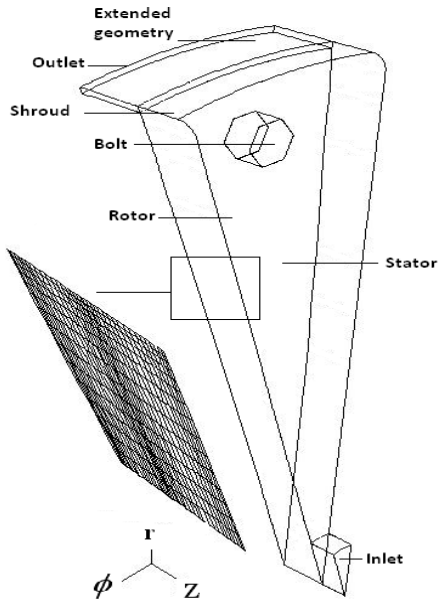
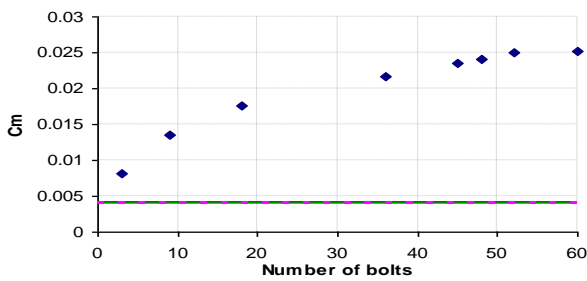


Figure 14. A Section of the Computational Mesh used for the Bolt Windage Test Rig

Figure 15. Variation of Moment Coefficient with Number of Bolts N. Comparison Between Numerical and Experimental Results for 3, 9 and 18 bolts and also a plain disc: $Re_\phi = 6.8 \times 10^6$, $C_w = 10^5$ ($\lambda_T = 0.35$)



◆ CFD result-different number of bolts
 — Plain disc-CFD results
 - - - Continuous ring-CFD results

Figure 16. Predicted Variation of Moment Coefficient with

Number of Bolts, N for $Re_\phi = 6.8 \times 10^6$, $C_w = 10^5$ ($\lambda_T = 0.35$).

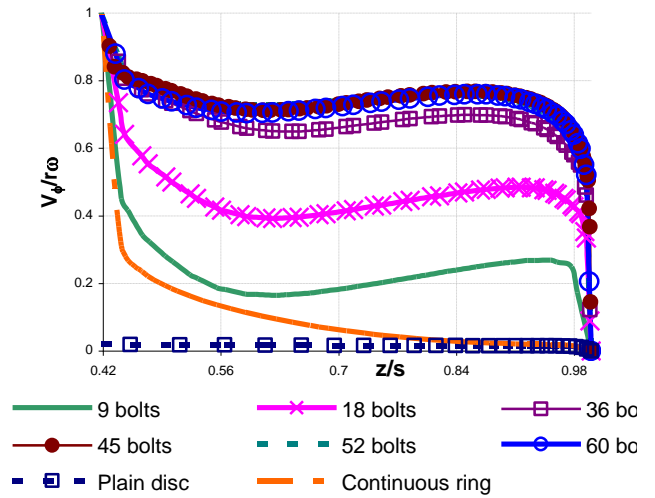


Figure 17. Predicted Axial Variation of Dimensionless Tangential Velocity at $r/b = 0.9$, $Re_\phi = 6.8 \times 10^6$ and $C_w = 10^5$ ($\lambda_T = 0.35$).

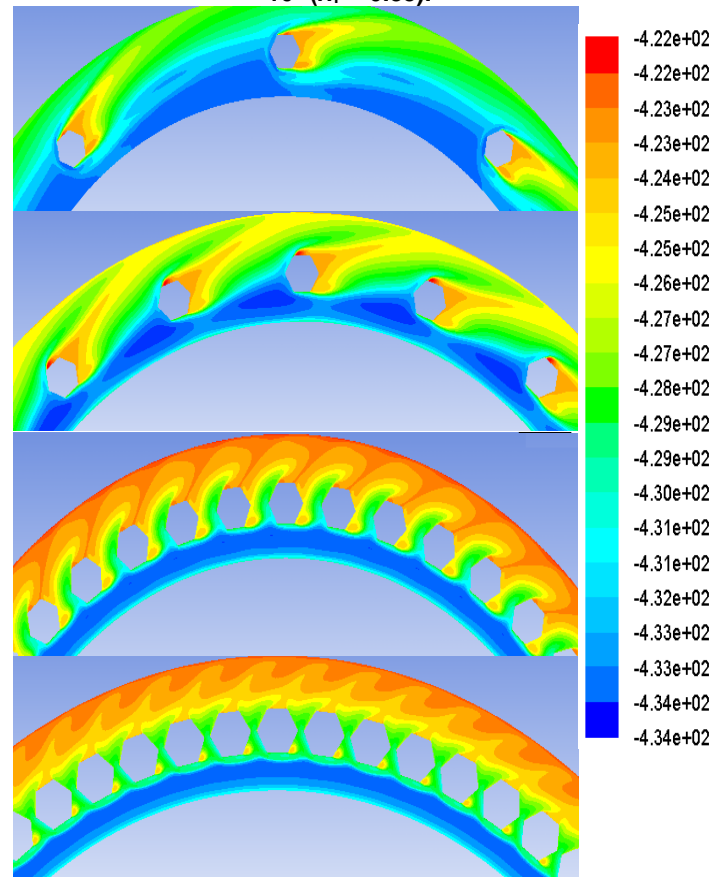


Figure 18. Entropy Contours around the Bolts for N = 9, 18, 45 and 60 ($Re_\phi = 6.8 \times 10^6$ and $C_w = 10^5$).

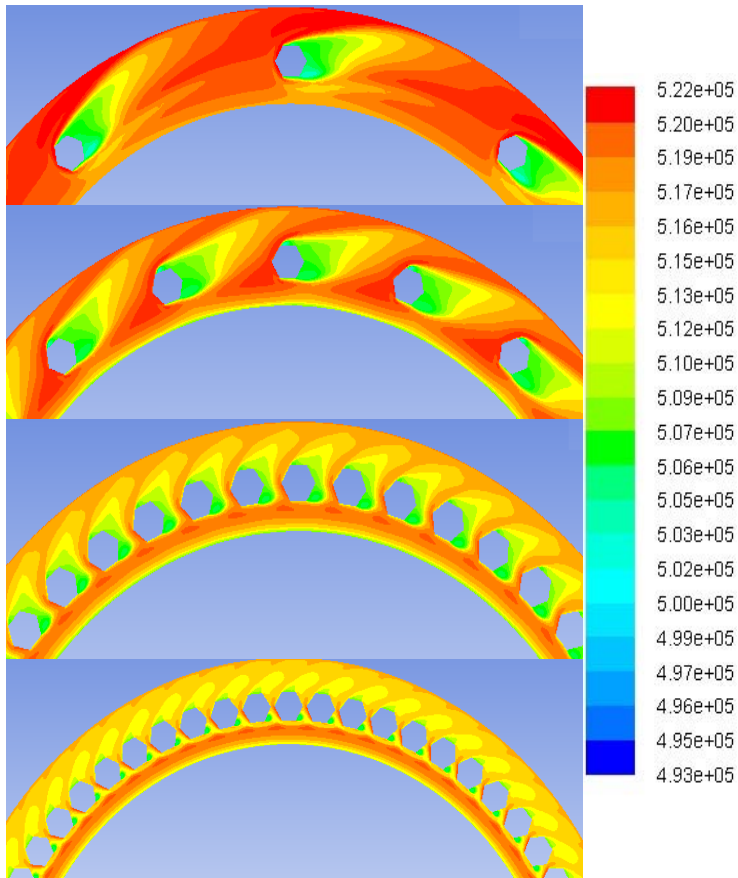


Figure 19. Relative total pressure Contours around the Bolts for $N = 9, 18, 45$ and 60 ($Re_\phi = 6.8 \times 10^6$ and $C_w = 10^5$).

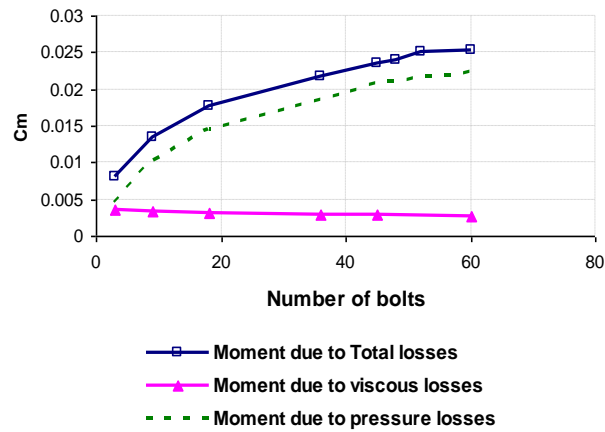


Figure 20. Variation of the overall moment coefficient, viscous and pressure-related (form drag and radial pumping) contributions with number of bolts ($Re_\phi = 6.8 \times 10^6$ and $C_w = 10^5$).

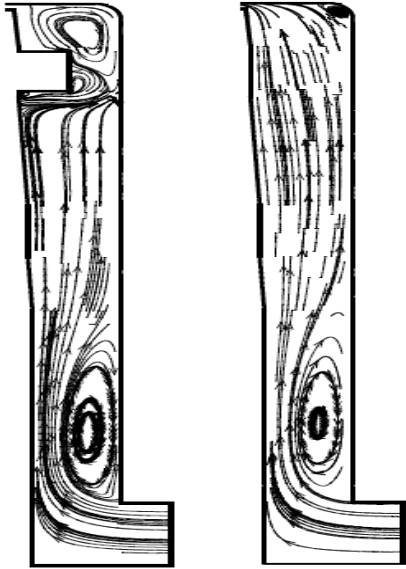


Figure 21. Velocity Streamlines for $Re_\phi = 6.8 \times 10^6$ and $C_w = 10^5$. Left: rotor-stator cavity with bolts ,Right: plain rotor-stator cavity

Table 2: Validation Test Case No. 2 Comparison between the moment coefficients of rotor for Different Turbulence Models

Model	Cm
Standard $k - \varepsilon$	0.00465
Realizable $k - \varepsilon$	0.00468
RNG $k - \varepsilon$	0.0047
Standard $k - \omega$	0.00435
SST $k - \omega$	0.00449
RSM	0.00509

Table 1: Validation Test Case No. 1 Comparison between the Tangential Velocity at $r/b=0.833$ and $z/s = 0.5$ for Different Turbulence Models

Model	$V_\phi / \omega r$
Experimental data	0.29
Standard $k - \varepsilon$	0.3538
Realizable $k - \varepsilon$	0.3522
RNG $k - \varepsilon$	0.3509
Standard $k - \omega$	0.339
SST $k - \omega$	0.34
RSM	0.37